High single-spatial-mode pulsed power from 980nm emitting diode lasers

Martin Hempel, Jens W. Tomm, Thomas Elsaesser, and Mauro Bettiati

Citation: Appl. Phys. Lett. **101**, 191105 (2012); doi: 10.1063/1.4766267
View online: http://dx.doi.org/10.1063/1.4766267
View Table of Contents: http://apl.aip.org/resource/1/APPLAB/v101/i19
Published by the American Institute of Physics.

High single-spatial-mode pulsed power from 980 nm emitting diode lasers

Martin Hempel,[1] Jens W. Tomm,[1] Thomas Elsaesser,[1] and Mauro Bettiati[2]
[1]*Max-Born-Institute für Nichtlineare Optik und Kurzzeitspektroskopie, Max-Born-Str. 2A, 12489 Berlin, Germany*
[2]*3S PHOTONICS, Route de Villejust, F-91625 Nozay Cedex, France*

(Received 21 August 2012; accepted 22 October 2012; published online 7 November 2012)

Single-spatial-mode pulsed powers as high as 13 W and 20 W in 150 and 50 ns pulses, respectively, are reported for 980 nm emitting lasers. In terms of energy, single-spatial-mode values of up to 2 μJ within 150 ns pulses are shown. In this high-power pulsed operation, the devices shield themselves from facet degradation, being the main degradation source in continuous wave (cw) operation. Our results pave the way towards additional applications while employing available standard devices, which have originally been designed as very reliable cw fiber pumps. © *2012 American Institute of Physics*. [http://dx.doi.org/10.1063/1.4766267]

High-power lasers for the 980 nm emission range have attracted a lot of interest, originally mainly for pumping of erbium doped fiber amplifiers in telecom applications.[1] Other applications joined, e.g., blue-green light sources for display and projection,[2] medical (surgery and genetic research), spectroscopy, remote sensing, laser radar, and also pure high-power generation. At least in part, this additional interest had a very plain background: The wavelength region around 980 nm represents the "best" for GaAs-based diode lasers in terms of absolute output power, conversion efficiency, and reliability. Most of today's record values are achieved with so-called "9XX nm emitting devices."[3,4] Additionally, large-lot production results in cost savings. Therefore, 980 nm emitting diode lasers are preferably employed in applications whenever possible.

High-power single-spatial-mode devices represent the most advanced devices in terms of brightness. Commercial device vendors quote typically 100–800 mW of reliable continuous wave (cw) emission powers in single-spatial-mode operation. However, depending on the complexity of device architectures, values of several W are achievable. Even higher power levels can be achieved if the devices are operated pulsed. This report is on the potential of high-end pump sources, which have originally been designed as highly reliable cw terrestrial pumps (750 mW), to operate in a high-power short pulse regime. This operation mode could enable additional applications as seed lasers in laser systems and for direct marking, e.g., through a fiber laser architecture. Demanding printing applications could also benefit.

Integrated emission powers as high as 30 W within pulses of 150 ns duration are achieved, while single-spatial-mode powers of 20 W can be maintained over 50 ns. In terms of energy, we demonstrate single-spatial-mode values of up to 2 μJ within 150 ns pulses.

This letter is organized as follows: After introducing the device architectures, we experimentally address their high-power limits including their degradation behavior during cw operation. Then, we come to pulsed excitation with ns-μs pulses. Actual power levels are achieved exceeding those the devices are specified for by nearly two orders of magnitude. In contrast to the cw situation, at highest emission powers the devices shield themselves from degradation. Our results pave the way towards additional applications while employing available standard devices.

Device structure and technology have been described in detail in an earlier paper.[5] We briefly recall here that the vertical laser structure has low internal losses (0.85 cm^{-1}) and low far-field angles of 6° × 18° (full width at half maximum) in the slow and fast-axes, respectively. The single spatial mode ridge waveguide is obtained by inductively coupled plasma etching on a full 3 in. wafer. The laser cavity is 3.9 mm in length. The chips are packaged *p*-side up to ceramic submounts, which are clamped onto a temperature-stabilized copper heat-sink; see Fig. 1(a). Threshold currents are in the 75 mA range, while typical emission powers are

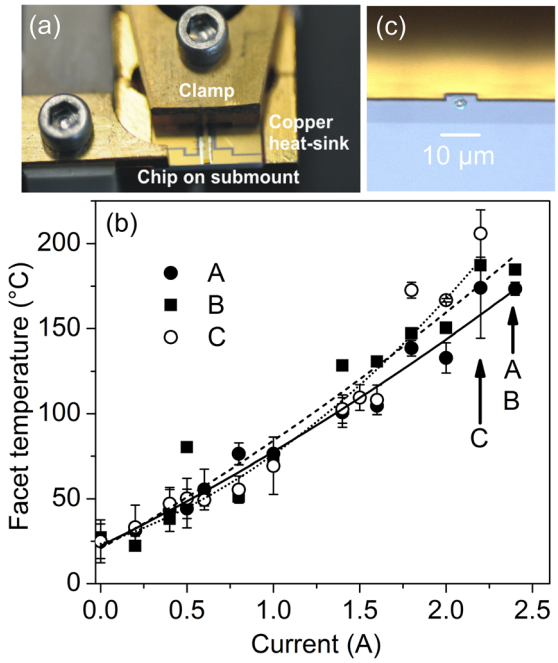

FIG. 1. (a) Chip on submount being clamped onto a temperature-stabilized copper heat-sink. (b) Averaged facet temperatures (symbols) vs. cw operation current for 3 device batches (A-C). The arrows mark the COMD thresholds (in terms of operation power) for the three batches, while the lines are best (second order polynomial) fits as guides to the eye. (c) Micrograph of the damage pattern at a device of batch B as created by COMD during cw operation. This type of signature is representative for all devices degraded during cw operation.

above 0.85 and 1.5 W at operation currents of 1 and 2 A, respectively. All light-emission-vs.-current characteristics (*L-I*) are "kink-free" up to ~1.8 A. Three batches of devices, referred to as A, B, and C have been tested with a total of 26 individual devices being involved.

During *cw-operation* front facet (surface) temperatures are measured by micro-Raman spectroscopy using a SI TriVista TR 557 spectrometer; for methodology, see Ref. 6. Typical measuring times for a single spectrum (temperature data point) are on the order of 100 s. Simultaneously, the facet is observed by a camera microscope. This allowed detecting any facet alterations or drops in emission power. All cw measurements have been carried out at stabilized heat-sink temperatures of $T_{hs} = (25.0 \pm 0.2)\,^{\circ}C$.

Pulsed operation is excited by a laser driver PicoLAS LDP-V 50–100 V3. For minimizing the rise times to 10 ns, the device is directly attached to the laser driver. Spatially and temporally resolved nearfields of the devices are monitored with a streak-camera (Haamatsu C1587) equipped with an optical microscope (100 × objective). Thermal emission (Planck's radiation) from the devices is monitored with a Thermosensorik CMT384 camera while using a band-pass filter for 3.5–6.0 μm. One pixel images a square of $\sim 8.8 \times 8.8\ \mu m^2$. The integration time of the camera is set to cover the entire pulse. Temporally resolved infrared radiation is detected by a fast detector Judson J15D22-M204-S250U-60 that ensures together with a fast preamplifier a time resolution of better than 100 ns. Filters form a bandpass that allows detecting in the 1.5–2.5 μm near infrared (NIR) spectral range. Pulsed measurements have been carried out at $T_{hs} = (25.0 \pm 0.2)\,^{\circ}C$ and $T_{hs} = (85.0 \pm 0.2)\,^{\circ}C$.

We start by summarizing the results of the cw tests at high emission power levels, which represent a base of the high-power experiments. While Fig. 1(a) gives the geometry of device, package, and clamp holder, Fig. 1(b) presents the averaged front facet temperatures versus operation current compiled from all devices investigated (5 per batch). When increasing the cw operation current in a *L-I*-like measurement, the devices typically failed by catastrophic optical mirror damage (COMD). Thus, this sudden mechanism represents the principal degradation mode during cw operation. The current, when this sudden degradation came in, is named "COMD-threshold" and is indicated in Fig. 1(b) by arrows. In terms of cw emission power, the COMD-thresholds for batches A, B, and C amount to about 1.7, 1.7, and 1.6 W, respectively. Generally, the COMD power threshold of these devices is somewhat higher (2.0–2.2 W).[5] The observed values around 1.6–1.7 W are attributed to the cumulated effect of the intrinsic dispersion on this parameter and a slightly higher thermal impedance in the actual measurement bench used for the specific measurements discussed in the following. The facet temperatures measured just before COMD do not differ notably. Thus for these devices, we do not see any increased facet temperatures as "early warning" of upcoming COMD events. Figure 1(c) shows the degradation pattern of a device from batch B (B1) as observed at the front facet by a conventional light microscope. This pattern represents the degradation signature being typical for all failed devices (from all batches). Since the damage pattern for all batches looks similar, we assume the same (high) temperature to be reached during COMD. Thus, the temperature increase between 180 °C and the high temperature, where the damage pattern is generated, takes place fast compared to the 100 s of measuring time required for micro-Raman spectroscopy. Furthermore, it is notable that we observe repeatedly facet temperatures as high as 180 °C in a long-term stable operation regime.

After having quantified the ultimate limits for standard cw operation, we proceed towards high-power pulsed operation. Here, we applied a "step test"[7] that involves testing with single pulses and stepwise increasing current amplitudes. Furthermore, we follow for analytical purposes each high-power pulse a low-power test pulse (1.6 A). By analyzing this data, one gets again something like a *L-I* measurement, with the main distinction that now each data point represents the (average) laser emission within one single pulse. Figure 2 shows typical results obtained for 150 ns pulse length. One of the devices (A1) reaches about 20 W ($T_{hs} = 25\,^{\circ}C$) before it goes into roll-over without any notable degradation at this point and beyond. Another device (A2) even reaches average powers of up to 30 W ($T_{hs} = 85\,^{\circ}C$). In order to determine the range, where single-spatial-mode operation is available, we directly monitor the spatio-temporal emission pattern (nearfield) with a streak-camera. Figure 3 shows selected data. At a current of 12.4 A (13.8 W), i.e., at >18 times of the specified power for safe cw operation, single-spatial-mode operation is available during the entire 150 ns pulse; see Figs. 3(a) and 3(b). This is proved by the Gaussian shape of the lateral mode profile. Full lines represent fits to Gaussians, while open circles represent experimental data. The average single-spatial-mode power at 12.4 A amounts to more than 13 W. For further increased operation currents, there is a tendency towards the presence of two or even three lateral modes; see Figs. 3(c) and 3(d). For currents as high as 22.5 A, single-spatial-mode operation is available for the first 50 ns of the pulse only. The actual power level within these 50 ns reaches 20 W. Figure 4(a) quantifies the transition from single-spatial-mode to multi-lateral-mode operation. As "single-mode time," we denote the time, where the lateral mode profile changes from one Gaussian to two resulting in a temporary top hat profile, e.g., at ~60 ns between the red and the green curves in

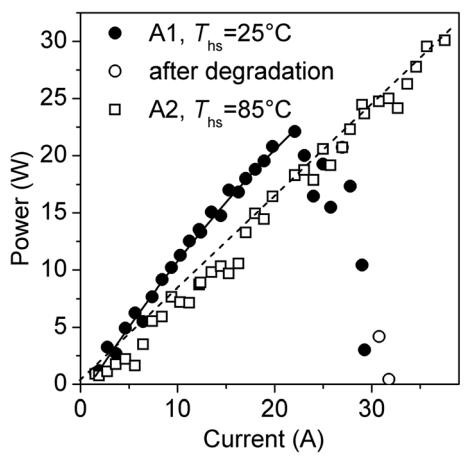

FIG. 2. Pulsed *L-I* curves for two devices. The pulse length is 150 ns, the peak pulse power is given.

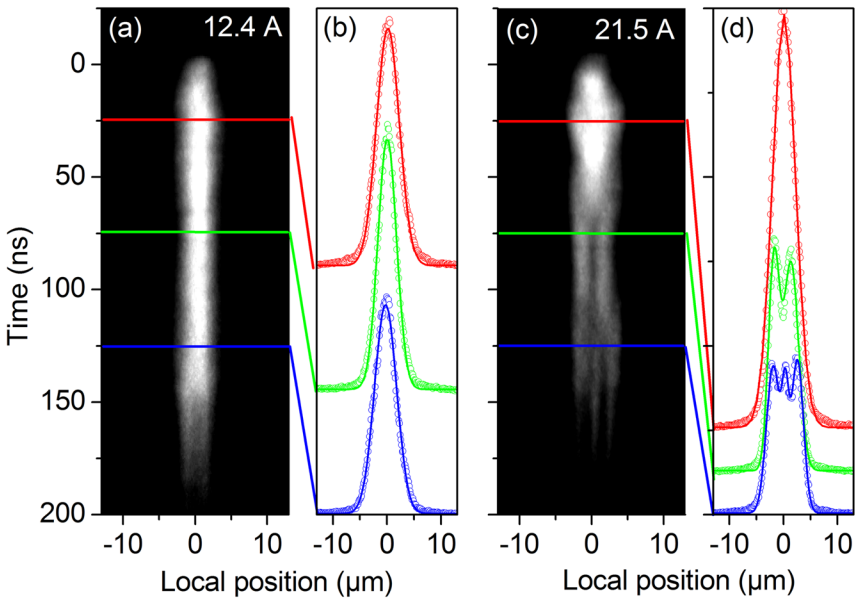

FIG. 3. Streak-camera traces (a) and (c) and cuts through these traces ((b) and (d), open circles) taken at the delay times marked ($T_{hs} = 25\,^{\circ}C$). Full lines in (b) and (d) represent Gaussian fits to the data.

Fig. 3(d), which are taken 25 and 75 ns after the pulses ignition, respectively. By considering the data shown in Fig. 4(a) and the *L-I*-curves, see Fig. 2, one can easily determine the energy, which is available in single-spatial-mode operation. Figure 4(b) presents the result. Up to 2 μJ is obtained in true single-spatial-mode operation ($T_{hs} = 25\,^{\circ}C$, $I = 13.6$ A), while 4.5 μJ are produced during operation with three lateral modes ($T_{hs} = 85\,^{\circ}C$, $I = 39.3$ A, see Fig. 2). When presenting Fig. 2, we already mentioned that device A1 went into (reversible) roll-over at $I \sim 20$ A. At $I \sim 30$ A, however, the same device irreversibly failed at a fairly low emission power level, as detected by analyzing the evolution of the test pulse pattern taken at 1.6 A after each pulse; see Figs. 4(c) and 4(d). The test pulse taken from device A1 after the pulse at $I = 29.3$ A, see Fig. 4(c), still looks similar to the one taken at lowest currents at the beginning of the test ($I = 1.6$ A), while the one taken after the pulse at $I = 30.7$ A, see Fig. 4(d), shows further power loss and the presence of five lateral modes. At this point, probably damage is created, which made the device re-ordering its internal mode structure even at lowest emission powers. Careful inspection of the device, however, revealed absolutely no externally visible degradation signature.

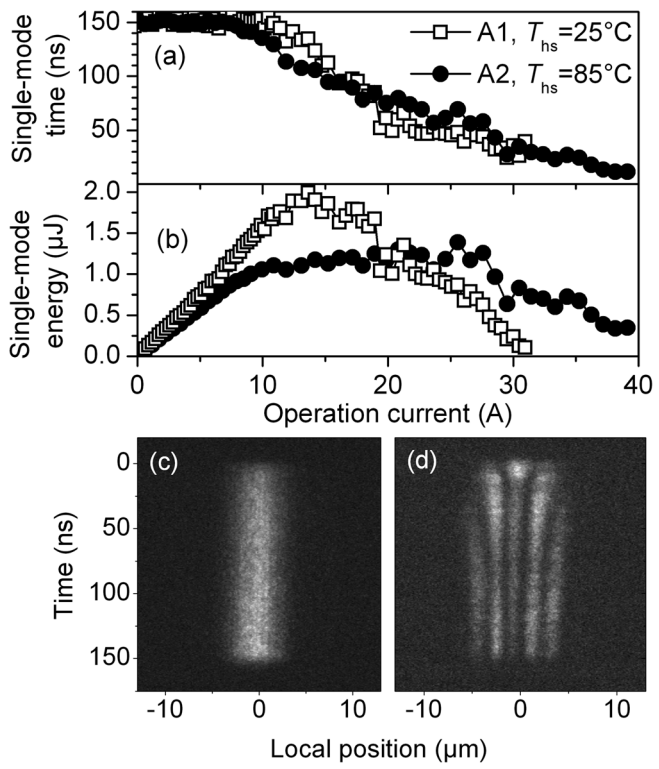

FIG. 4. (a) Time during which single-spatial-mode operation is maintained ("single mode time") during 150 ns current pulses. Data for longer pulses are not determined, however, "kink-free" cw operation until 1.8 A indicates this value for "infinite" pulse length. (b) Energy generated in true single-spatial-mode operation ("single mode energy") while operating the device with 150 ns current pulses. (c) and (d) Streak-camera traces taken in $I = 1.6$ A test pulses, which have been taken after $I = 29.3$ (c) and $I = 30.7$ A, (d) high-power pulses. ($T_{hs} = 25\,^{\circ}C$). While the data shown in (c) look almost similar as the one taken after the first pulse of $I = 1.6$ A, the one shown in (d) shows power loss and the presence of five lateral modes; i.e., a completely modified lateral mode structure even at very low powers.

In order to employ the before demonstrated potential of the pulsed operation regime for any application, the mechanisms setting the ultimate limits of operation must be revealed. This calls for additional experiments in order to *in situ* monitor the degradation. For this purpose, the test bed depicted in Fig. 5(a) has been assembled. While the diode laser again undergoes a step test sequence with increasing current amplitudes, we monitor the emission power transient from the front facet by a fast photodiode (PD) and infrared emission by a fast NIR detector. Both contributions are separated by a dichroic beamsplitter (BS), while filters in front of the detectors ensure to pick up the right spectral range. The side of the device is monitored by a thermocamera. Several devices underwent step tests by changing the pulse length between 50 ns and 9 μs.

Provocation of sudden degradation became only possible when switching to very long pulses, namely 9 μs, i.e., to 60× longer pulses than used in the preceding experiments. Figures 5(b)–5(d) show the data obtained from device A3 in a step test at $I = 8.2$ A (b) and (d) and $I = 8.7$ A (c). The initial degradation event took place after about 7.8 μs in the $I = 8.2$ A pulse; see arrow in Fig. 5(d). The abruptly dropping

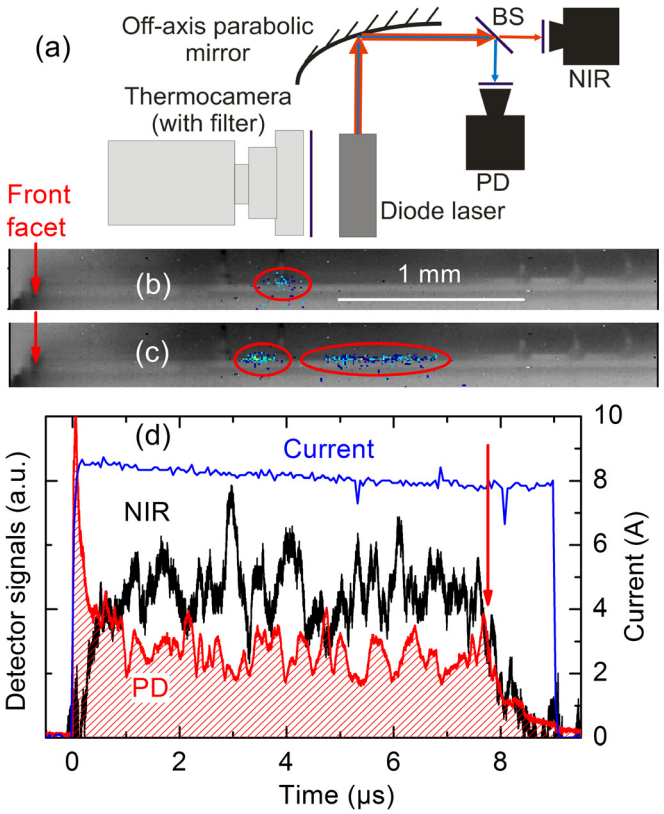

FIG. 5. (a) Test bed for *in situ* monitoring of the degradation of single-spatial-mode diode lasers. The emission from the front facet of the device is split (dichroic BS) into two fractions monitored with two separate detectors. While the device emission (~980 nm) is detected by a PD the spontaneous NIR emission is detected in the 1.5-2.5 μm spectral range. In contrast to these detectors, the thermocamera looks from the side towards the laser cavity. (b) and (c) Composite thermal images taken from the side of the devices during two high-power current pulses of $I = 8.2$ A (b) and $I = 8.7$ A (c) of 9 μs duration. Each of the images consists of two parts: There is an emissivity contrast image, which reveals the device geometry, see, e.g., bond wires on top. This image is taken without device operation (black/white contrast, integration time 1 ms), while the color-coded overlayed image reveals the thermal radiation (integration time 10 μs, see red ellipses). (d) Transient data taken during the high-power current pulses of $I = 8.2$ A of 9 μs duration; see also data presented in (b). The red arrow marks the degradation event involving the sudden PD- and NIR-signal collapses.

laser power (PD-signal) is accompanied by a weak thermal signature deep inside the laser cavity about 1.2 mm behind the laser facet; see marked area in Fig. 5(b). In the following $I = 8.7$ A pulse, two even more extended thermal signatures are observed, which are shifted compared to the initial one. During this pulse, the emission power detected by PD and NIR detectors was already very low. Thus, we conclude that this device degraded because of a thermal overload within the waveguide at its probably weakest location without producing COMD at any facet. Since the hotspot location is moving along the laser axis from one pulse to the next, cf. the highlighted areas in Figs. 5(b) and 5(c), a defect network spread as known for COMD is highly likely. This, however, takes place without affecting the facets mirror.

The PD- and NIR-traces reveal additional details about what happens in the interior of the device during the long μs pulse. When considering the PD-signal (red line), it should be kept in mind that the fluctuation is a true output power variation and not related to any noise. Although we investigated the "single-mode time" versus operation current in detail for shorter pulses only, cf. Fig. 4(a), it is clear that the observed emission power fluctuation is due to spatial mode hopping within (and around) the waveguide being still not fully thermalized on this timescale. The NIR-signal, on the other hand, represents a "defect photoluminescence" created in the substrate,[8] which is excited by laser emission that is transferred from the waveguide into its vicinity including the substrate. This happens, e.g., if multiple spatial modes do not fit into the waveguide that is designed for single-spatial-mode operation. Thus, the NIR-signal is roughly indicative for the fraction of laser power that remains within the device. Therefore, PD- and NIR-signals are predominantly anticorrelated (not always, since the laser light is also the only source for exciting the "defect photoluminescence"). The amplitude fluctuation of the PD signal amounts to >30% of the average amplitude (averaged in the 1–7 μs range), which is about 2.5 W. Thus, in this operation regime, there is a heat source near the waveguide, in which more than 700 mW of power is redistributed on a sub-μs timescale in an uncontrolled way. Eventually, this leads to device degradation. This shows also the limits of the applicability of the pulsed operation. It works well in single-spatial-mode operation with short pulses. Here, the transition to multi lateral modes even protects the device from COMD. But on a timescale of several μs, these benefits get lost and the device becomes thermally unstable. The great advantage of short pulse operation, namely the power enhancement by two orders of magnitude works only as long as single-spatial-mode operation is maintained.

It is worthwhile to address another implication of our initial experiments with cw excitation: In the literature, a critical temperature $T_{crit} = 120°–160°$ is quoted to be distinctive for the ignition of COMD, which after that takes place on a very short timescale.[7] Obviously, our devices exceed this T_{crit}-value by showing long-term stable facet temperatures as high as ~180 °C. We consider this experimental fact first of all an indication for the ability of our devices to withstand such high facet temperatures. The wide spread in T_{crit}-values, however, indicates also that T_{crit} depends on technology (passivation, protection, coating) and earlier reported lower values around 120 °C (for an overview see Ref. 7) rather describe early stages of facet processing.

In summary, we present a complementary study of the behavior of single-spatial-mode mode pump sources operated close to their power limits in pulsed and cw operation. 30 W of power within pulses of 150 ns are achieved, while single-spatial-mode powers of 20 W can be maintained over 50 ns. In terms of energy, we demonstrate single-spatial-mode values of up to 2 μJ within 150 ns pulses. If the pulse lengths do not exceed several 100 ns, the devices protect their facets themselves from COMD by switching into multi-lateral-mode-operation, which is accompanied by substantial power loss. Our results pave the way for additional applications while employing available standard devices.

[1]T. Pliska, S. Arlt, R. Battig, T. Kellner, I. Jung, N. Matuschek, P. Mauron, B. Mayer, S. Mohrdiek, E. Muller, S. Pawlik, H. U. Pfeiffer, B. Schmidt, B. Sverdlov, S. Teodoropol, J. Troger, B. Valk, and C. Harder, Opt. Lasers Eng. **43**(3–5), 271 (2005).
[2]A. Jechow, R. Menzel, K. Paschke, and G. Erbert, Laser Photonics Rev. **4**(5), 633 (2010).

[3]N. Lichtenstein, M. Krejci, Y. Manz, J. Boucart, B. Valk, J. Muller, C. Button, S. Weiss, S. Pawlik, and B. Sverdlov, Proc. SPIE **6876**, 68760C (2008).
[4]I. B. Petrescu-Prahova, P. Modak, E. Goutain, D. Silan, D. Bambrick, J. Riordan, T. Moritz, S. D. McDougall, B. Qiu, and J. H. Marsh, Proc. SPIE **7198**, 71981I (2009).
[5]M. A. Bettiati, C. Starck, F. Laruelle, V. Cargemel, P. Pagnod, P. Garabedian, D. Keller, G. Ughetto, J.-C. Bertreux, L. Raymond, G. Gelly, and R.-M. Capella, Proc. SPIE **6104**, 61040F (2006).
[6]T. J. Ochalski, D. Pierscinska, K. Pierscinski, M. Bugajski, J. W. Tomm, T. Grunske, and A. Kozlowska, Appl. Phys. Lett. **89**(7), 071104 (2006).
[7]J. W. Tomm, M. Ziegler, M. Hempel, and T. Elsaesser, Laser Photonics Rev. **5**(3), 422 (2011).
[8]M. Ziegler, R. Pomraenke, M. Felger, J. W. Tomm, P. Vasa, C. Lienau, M. BouSanayeh, A. Gomez-Iglesias, M. Reufer, F. Bugge, and G. Erbert, Appl. Phys. Lett. **93**(4), 041101 (2008).